Oxidative DNA damage induces the ATM-mediated transcriptional suppression of the Wnt inhibitor WIF-1 in systemic sclerosis and fibrosis

Silvia Svegliati, Giusi Marrone, Antonio Pezone, Tatiana Spadoni, Antonella Grieco, Gianluca Moroncini, Domenico Grieco, Maria Vinciguerra, Savina Agnese, Astrid Jüngel, Oliver Distler, Anna Maria Musti, Armando Gabrielli and Enrico V. Avvedimento

(September 2, 2014)
Science Signaling **7** (341), ra84. [doi: 10.1126/scisignal.2004592]

PHYSIOLOGY

Oxidative DNA damage induces the ATM-mediated transcriptional suppression of the Wnt inhibitor WIF-1 in systemic sclerosis and fibrosis

Silvia Svegliati,[1]* Giusi Marrone,[2]* Antonio Pezone,[2]* Tatiana Spadoni,[1] Antonella Grieco,[1] Gianluca Moroncini,[1,3] Domenico Grieco,[2] Maria Vinciguerra,[4] Savina Agnese,[2] Astrid Jüngel,[5] Oliver Distler,[5] Anna Maria Musti,[6] Armando Gabrielli,[1,3]† Enrico V. Avvedimento[2]†

Systemic sclerosis (SSc) is an autoimmune disease characterized by extensive visceral organ and skin fibrosis. SSc patients have increased production of autoreactive antibodies and Wnt signaling activity. We found that expression of the gene encoding Wnt inhibitor factor 1 (WIF-1) was decreased in fibroblasts from SSc patient biopsies. WIF-1 deficiency in SSc patient cells correlated with increased abundance of the Wnt effector β-catenin and the production of collagen. Knocking down WIF-1 in normal fibroblasts increased Wnt signaling and collagen production. WIF-1 loss and DNA damage were induced in normal fibroblasts by either SSc patient immunoglobulins or oxidative DNA-damaging agents, such as ultraviolet light, hydrogen peroxide, or bleomycin. The DNA damage checkpoint kinase ataxia telangiectasia mutated (ATM) mediated WIF-1 silencing through the phosphorylation of the transcription factor c-Jun, which in turn activated the expression of the gene encoding activating transcription factor 3 (ATF3). ATF3 and c-Jun were recruited together with histone deacetylase 3 (HDAC3) to the *WIF-1* promoter and inhibited *WIF-1* expression. Preventing the accumulation of reactive oxygen species or inhibiting the activation of ATM, c-Jun, or HDACs restored *WIF-1* expression in cultured SSc patient cells. Trichostatin A, an HDAC inhibitor, prevented WIF-1 loss, β-catenin induction, and collagen accumulation in an experimental fibrosis model. Our findings suggest that oxidative DNA damage induced by SSc autoreactive antibodies enables Wnt activation that contributes to fibrosis.

INTRODUCTION

The Wnt (Wingless) family is a group of highly conserved secreted proteins that regulate cell-to-cell interactions during embryogenesis and is implicated in carcinogenesis, aging, and fibrosis (*1*). To be effective during embryogenesis and stem cell differentiation, Wnt signals need to be carefully controlled temporally and spatially (*2*). This is accomplished by a balance of Wnt-activating proteins or Wnt-inhibiting proteins [for a review, see (*3*)]. Specifically, inhibitors either bind directly to Wnt, such as Wnt inhibitory factor 1 (WIF-1), or interact with the Wnt receptor complex (*4*).

WIF-1 is a highly conserved gene containing a unique Wnt inhibitory domain and five epidermal growth factor (EGF)–like repeat domains. WIF-1 inhibits Wnt signaling during development (*5*), and it is silenced during the neoplastic progression of various human cancers (*6*, *7*). Increased Wnt signaling is also linked to mesenchymal differentiation and tissue-specific cellular aging. Unrestrained Wnt signaling decreases the pool of mesenchymal stem cells and ultimately induces fibrosis (*8*). Systemic sclerosis (SSc) is a disease characterized by extensive tissue fibrosis, and Wnt–β-catenin signaling is a key player in fibroblast activation and tissue fibrosis in SSc (*9*). We previously showed that fibroblasts derived from SSc patients undergo senescence prematurely because of extensive oxidative stress and DNA damage. This phenotype is induced in normal cells through constitutive activation of platelet-derived growth factor receptor (PDGFR) signaling by agonistic autoreactive antibodies (*10*, *11*), but the specific mechanism leading to Wnt activation in SSc cells is not yet clear. Notably, Wnt activation has different consequences on the fate of epithelial and mesenchymal cells: DNA damage promotes transformation or death in epithelial cells (*12*) but accelerates aging and increases collagen abundance in mesenchymal cells (*8*, *13*). Therefore, we investigated the mechanism linking the effects of SSc patient–derived immunoglobulins with the induction of Wnt signaling in either normal or SSc patient fibroblasts derived from skin biopsies.

RESULTS

WIF-1 is silenced in SSc patient fibroblasts by promoter histone deacetylation

Wnt signaling is increased in the skin and fibroblasts of SSc patients compared with the same samples derived from normal subjects (*9*, *13*), suggesting that either the activity of proteins that stimulate the pathway is increased or that of proteins which inhibit Wnt signaling is decreased. We found that the abundance of the secreted Wnt inhibitor, WIF-1, was decreased in skin biopsies from SSc patients compared with normal cultured fibroblasts (Fig. 1, A to C, and fig. S1A). Immunofluorescence detection of WIF-1 in SSc patient fibroblasts further confirmed significantly decreased WIF-1 abundance, as well as a concomitant increase in that of β-catenin (Fig. 1D), which is a marker of canonical Wnt signaling. Because *WIF-1* is silenced in breast cancer cells by methylation of its promoter (*14*),

[1]Dipartimento di Scienze Cliniche e Molecolari, Clinica Medica, Università Politecnica delle Marche, 60126 Ancona, Italy. [2]Dipartimento di Medicina Molecolare e Biotecnologie Mediche, Università degli Studi di napoli Federico II, 80132 Naples, Italy. [3]Dipartimento di Medicina Interna, Ospedali Riuniti, 60126 Ancona, Italy. [4]Cancer Research UK, Clare Hall, London EN6 3LD, UK. [5]Center of Experimental Rheumatology, Department of Rheumatology, University Hospital Zurich, 8091 Zurich, Switzerland. [6]Dipartimento di Farmacia e Scienze della Salute e della Nutrizione, Università della Calabria, Arcavacata di Rende (CS) 87036, Italy.
*These authors contributed equally to this work.
†Corresponding author. E-mail: avvedim@unina.it (E.V.A.); a.gabrielli@univpm.it (A.G.)

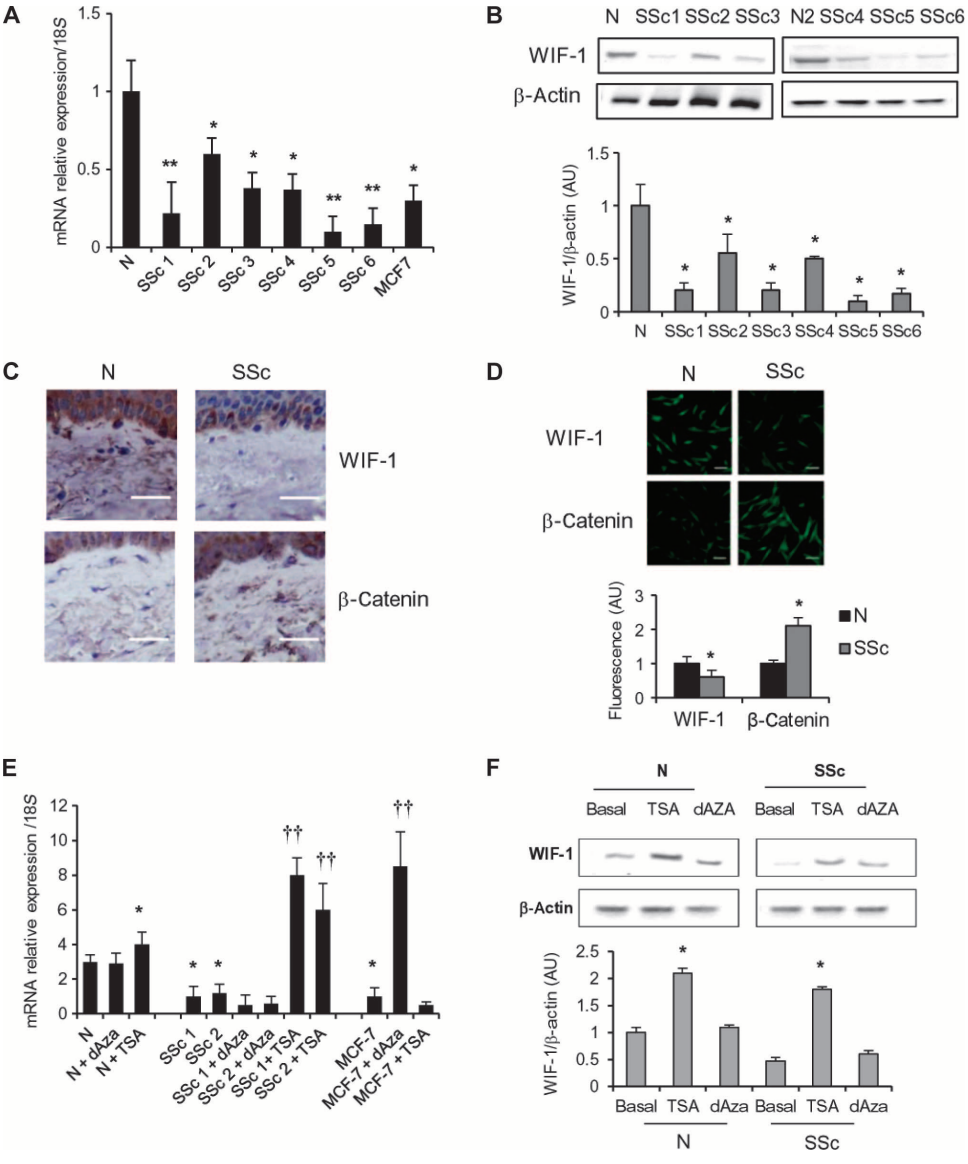

Fig. 1. Silencing of WIF-1 in fibroblasts from SSc and in breast cancer cells (MCF7). (**A**) Reverse transcription polymerase chain reaction (RT-PCR) for *WIF-1* mRNA abundance in serum-starved primary fibroblasts from six normal subjects (N, means ± SD from fig. S1A) or six SSc patients compared with MCF7 cells. Data are means ± SD from three independent experiments normalized to 18*S* RNA abundance. (**B**) Western blot for WIF-1 in whole-cell lysates from six SSc patients compared with normal samples. Data are means ± SD from three independent cultures from each patient. AU, arbitrary unit. (**C**) Representative immunohistochemistry for WIF-1 and β-catenin in skin biopsies from three SSc and three normal subjects. Scale bars, 100 μm. (**D**) Confocal microscopy for WIF-1 and β-catenin in SSc or normal fibroblasts. Data are means ± SD of at least 50 cells per field from six SSc patients and six normal subjects. Scale bars, 100 μm. (**E** and **F**) Analysis of *WIF-1* expression (E) and WIF-1 abundance (F) in normal or SSc fibroblasts (from six patients each) and MCF7 cells treated with 300 nM TSA or 4 μM 5-azacytidine for 24 hours. Data are means ± SD of three independent experiments. $^{*}P < 0.05$, $^{**}P < 0.01$ compared to normal control; $^{\dagger\dagger}P < 0.01$ compared to SSc.

and because the abundance of *WIF-1* mRNA in a culture of MCF7 breast cancer cells was similar to that in SSc patient fibroblasts (Fig. 1A), we hypothesized that the same may be true in SSc patient cells. However, in contrast to that in MCF7 cells, the *WIF-1* gene was not methylated in SSc patient fibroblasts as assessed by bisulphite sequencing (fig. S1B), and its expression was not restored by treatment with 5-azacytidine, a demethylating agent (Fig. 1E). It was, however, restored and further increased by treatment with the histone deacetylase (HDAC) inhibitor trichostatin A (TSA) at both the mRNA and protein levels (Fig. 1, E and F). In contrast, the expression of *WIF-1* was restored in MCF7 cells only by 5-azacytidine (Fig. 1E), indicating that whereas the loss of WIF-1 may be caused by DNA methylation in breast cancer epithelia, its loss is caused by histone deacetylation in SSc patient fibroblasts.

WIF-1 silencing enhances Wnt activity and induces *COL1A1* expression

To investigate the consequences of decreased *WIF-1* expression in SSc cells, we silenced *WIF-1* in normal fibroblasts using targeted silencing RNAs (siRNAs) and measured the transcript abundance of *COL1A1* (encoding collagen type 1 α 1) and *CTNNB1* (encoding β-catenin). Loss of WIF-1 initially increased the expression of *CTNNB1* (Fig. 2A). The abundance of β-catenin at both the transcriptional and translational levels was inversely correlated with WIF-1 abundance (Fig. 2A and fig. S2A), possibly because of the stabilizing effects of Wnt on β-catenin (*15*). *COL1A1* mRNA, however, increased only 96 hours after WIF-1 siRNA transfection, suggesting an indirect effect of *WIF-1* on *COL1A1* gene expression (Fig. 2A). We noticed a significant and unexpected early inhibition of *COL1A1* expression in the first 48 hours after transfection with *WIF-1* siRNA (Fig. 2A). We speculate that in the absence of certain growth factors [such as platelet-derived growth factor (PDGF), which induces collagen synthesis (*10*)], a rapid increase of β-catenin may inhibit rather than stimulate *COL1A1* expression.

To this end, we analyzed the effects of WIF-1 depletion in cells stimulated with PDGF. Loss of WIF-1 at 72 to 96 hours increased the basal expression of *COL1A1* and prevented PDGF-induced expression of *COL1A1* (Fig. 2, B and C), suggesting that cells with low abundance of WIF-1 (such as SSc cells) express increased *COL1A1* and are thus refractory to collagen-inducing signals. Decreased WIF-1 correlated with the induction of β-catenin and T cell factor (TCF)–dependent transcription in SSc patient cells, as assessed with a luciferase reporter (fig. S2B), as well as high abundance of β-catenin in idiopathic lung fibrosis cells (fig. S2C) (*16*), which is also evident in other fibrotic tissues (*17*, *18*).

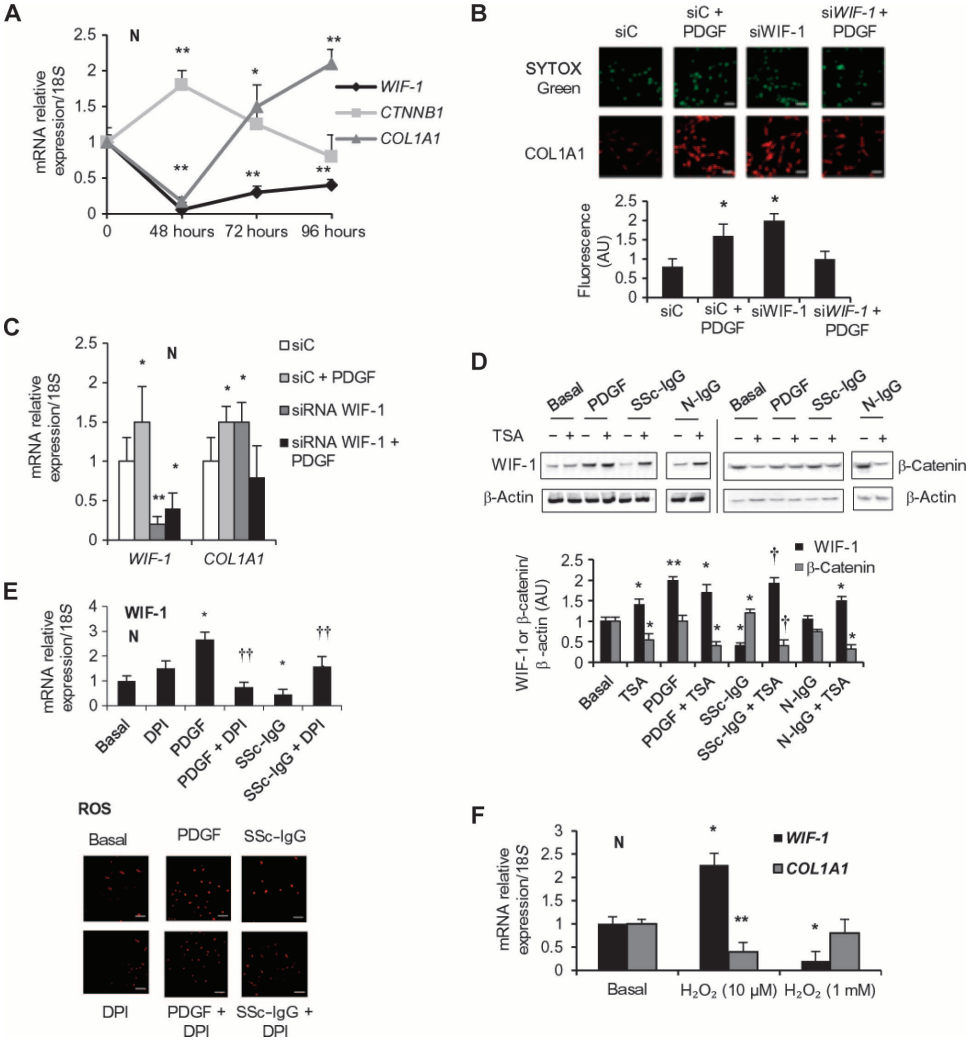

Fig. 2. WIF-1 silencing amplifies Wnt signaling and induces COL1A1 expression. (A) Normal fibroblasts were transiently transfected with scrambled or WIF-1–targeted siRNA (siWIF-1). At the indicated times, the relative expression of endogenous *WIF-1*, *CTNNB1*, and *COL1A1* was measured by RT-PCR. (B) Representative immunofluorescence staining for COL1A1 in control-transfected (siC) or WIF-1–silenced cells (siWIF-1) for 48 hours, and then stimulated with PDGF (15 ng/ml) for 24 hours. Images were captured at 72 hours after transfection. (C) RT-PCR analysis of *COL1A1* and *WIF-1* mRNA in fibroblasts treated as in (B). (D) WIF-1 and β-catenin immunoblot in serum-starved normal fibroblasts pretreated with TSA (300 nM, 1 hour) and then stimulated with PDGF (15 ng/ml, 24 hours) or IgG isolated from three SSc or normal subjects (200 μg/ml, 24 hours). (E) *WIF-1* mRNA abundance (upper panel) and ROS detection (lower panel) of fibroblasts not treated (basal) or pretreated with DPI (10 μM, 1 hour) and then stimulated with PDGF (15 ng/ml) or immunoglobulin isolated from three distinct SSc patients (SSc-IgG) (200 μg/ml) for 24 hours. (F) *WIF-1* and *COL1A1* mRNA abundance in serum-starved normal fibroblasts treated with H_2O_2 (10 μM or 1 mM for 2 hours). Data in (A) to (F) are means ± SD of three independent experiments. $^{*}P < 0.05$, $^{**}P < 0.01$ compared to controls; $^{\dagger}P < 0.01$ compared to SSc-IgG–treated sample (D); $^{\dagger\dagger}P < 0.01$ compared to PDGF-treated sample (E).

Persistent oxidative stress silences WIF-1

To investigate the mechanism that silenced WIF-1, the abundance of WIF-1 and β-catenin was measured in normal fibroblasts exposed to recombinant PDGF or immunoglobulins isolated from normal volunteers (N-IgG) or SSc patients (SSc-IgG). After 24 hours in PDGF, the abundance of WIF-1 increased and that of β-catenin did not change in normal fibroblasts (Fig. 2D). In contrast, exposure to SSc-IgG, but not N-IgG, decreased WIF-1 and increased β-catenin protein abundance. Fibroblasts lacking functional PDGFR showed no changes in either *WIF-1* or *COL1A1* transcript abundance in response to PDGF or SSc-IgG, whereas reconstitution of PDGFR restored the effects of both PDGF and SSc-IgG on *WIF-1* expression and increased the expression of *COL1A1* (fig. S2D). This suggested that although PDGF and SSc-IgG had opposite effects on the abundance of WIF-1, they appeared to act through the same receptor. To rule out possible artifacts caused by contaminants in SSc-IgG fractions and to demonstrate the biological activity of SSc-IgG on *WIF-1* expression, we tested a recombinant IgG (immunoglobulin G) targeting PDGF that was cloned from lymphocytes of a scleroderma patient. This IgG reduced *WIF-1* expression (fig. S2E). Because inhibition of HDAC by TSA reactivated *WIF-1* expression in SSc cells, we tested whether TSA inhibited SSc-IgG effects. TSA not only reverted the effects of SSc-IgG in normal fibroblasts but also markedly stimulated the expression of *WIF-1* and reduced β-catenin content (Fig. 2D), suggesting that HDAC is a target of the action of SSc-IgG.

To identify the targets of PDGF and SSc-IgG in altering *WIF-1* expression, we inhibited reactive oxygen species (ROS), which mediates the induction of *COL1A1* expression by PDGF or SSc-IgG (*10*). Depletion of ROS by diphenyleneiodonium (DPI), a general inhibitor of ROS-producing flavoenzymes (fig. S3) (*19*), prevented the effects of either PDGF or SSc-IgG on the expression of *WIF-1* (Fig. 2E). Normal fibroblasts exposed to increasing H_2O_2 concentrations differentially affected the expression of *WIF-1*, depending on the time and the concentrations used. Whereas addition of 10 μM H_2O_2 for 2 hours increased *WIF-1* expression, exposure to 1 mM H_2O_2 for 2 hours significantly decreased it compared to basal expression (Fig. 2F). Low H_2O_2 mimicked the effects of PDGF (induced *WIF-1* expression), whereas high H_2O_2 replicated SSc-IgG action (inhibited *WIF-1* expression). We note that ROS induced by PDGF are transient and rapid, whereas ROS induced by SSc-IgG are prolonged (*11*); this may explain why only high H_2O_2 inhibited *WIF*-1 expression in normal cells. In SSc cells, ROS persist longer even in the absence of serum or exogenous SSc-IgG because they sustain an autoamplification loop involving active extracellular signal–regulated kinase 1 and 2 (ERK1/2) and NADPH (reduced form of nicotinamide adenine dinucleotide phosphate) oxidase (*10*).

Collectively, the data suggest that WIF-1 silencing induced by high or persistent ROS exposure promotes Wnt signals to respond to oxidative stress.

DNA damage and checkpoint kinase ataxia telangiectasia mutated silence WIF-1

Persistent oxidative stress, caused by H_2O_2 or ultraviolet (UV) light, for example, can induce DNA damage and activation of ataxia telangiectasia mutated (ATM) and the DNA damage response (DDR) (*20*). SSc patient–derived fibroblasts and normal fibroblasts treated with high concentrations of H_2O_2 displayed conspicuous DNA damage, evident by the accumulation of phosphorylated ATM (Fig. 3, A and B) and phosphorylated p53 binding protein 1 (53BP1) (Fig. 3C), hallmarks of the DDR (*20*). In SSc fibroblasts, inhibiting ATM with the competitive inhibitor KU55933 (KuDOS 55933) increased *WIF-1* expression and reduced *COL1A1* expression compared to that seen in normal cells (Fig. 3D). Similarly, DNA damage induced by UV light in normal fibroblasts reduced *WIF-1* mRNA abundance (Fig. 3E). Treatment with the ATM inhibitor not only prevented UV-induced repression of *WIF-1* but also increased it basally (Fig. 3E). The expression of other genes that encode inhibitors of Wnt signaling, such as axis inhibition protein 2, secreted frizzled-related protein, and glycogen synthase kinase 3 was also inhibited by UV, but was not dependent on ATM (fig. S4), suggesting that WIF-1 might be a specific target in the ATM-induced damage response.

To examine whether *WIF-1* expression was inhibited by ROS and ATM through a single mechanism, we treated normal or A-T fibroblasts (GM05823) with 250 μM H_2O_2, which was sufficient to reduce *WIF-1* expression in wild-type fibroblasts (Fig. 3F). However, in A-T fibroblasts, the same concentration of H_2O_2 did not significantly affect *WIF-1* expression (Fig. 3F). Exposure of normal fibroblasts to higher concentrations (1 mM) of H_2O_2 silenced *WIF-1* expression and (as confirmation of the functional effects on Wnt signaling) stimulated β-catenin abundance, but not in the presence of the ATM inhibitor (fig. S5), indicating that ATM was downstream of ROS induction and mediated the repression of *WIF-1* expression. This finding agrees with evidence that ATM can be directly activated by ROS independently of the DDR-initiating MRE11-RAD50-NBS1 (MRN) complex (*20*). However, to test whether WIF-1 silencing was

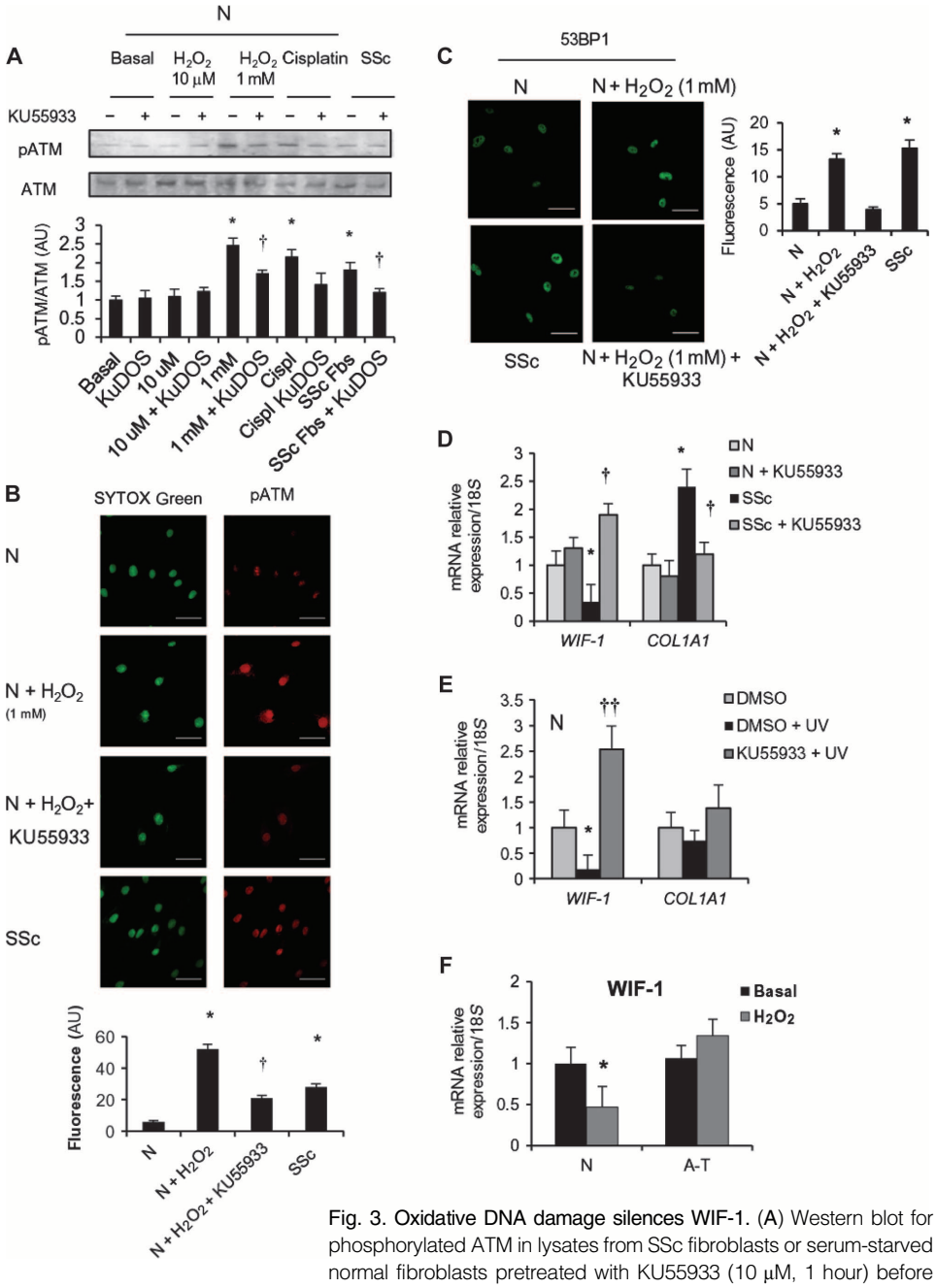

Fig. 3. Oxidative DNA damage silences WIF-1. (**A**) Western blot for phosphorylated ATM in lysates from SSc fibroblasts or serum-starved normal fibroblasts pretreated with KU55933 (10 μM, 1 hour) before H_2O_2 (10 μM and 1 mM, 2 hours) or cisplatin (5 μM, 24hours). Blots are representative of three independent experiments. (**B**) Phosphorylated ATM (Ser^{1981}; red) and DNA (SYTOX Green) in normal or SSc fibroblasts pretreated with KU55933 (10 μM, 1 hour), and then treated with H_2O_2 (1 mM, 30 min). Images are representative of four independent experiments. Scale bars, 100 μm. (**C**) Cells treated as in (A) and stained for 53BP1. Images are representative of four independent experiments. Scale bars, 100 μm. (**D**) *WIF-1* and *COL1A1* mRNA expression in normal (N) and SSc fibroblasts in the presence or absence of KU55933 (10 μM, 1 hour). (**E**) *WIF-1* and *COL1A1* mRNA abundance in normal fibroblasts pretreated with 10 μM KU55933 and then exposed to UV (80 J/m^2). DMSO, dimethyl sulfoxide. (**F**) *WIF-1* expression in serum-starved A-T or normal (N) fibroblasts after H_2O_2 treatment (250 μM, 30 min). Data in (A) to (F) are means ± SD of three independent experiments. $^*P < 0.01$ compared to basal or control; $^{\dagger}P < 0.05$ compared to H_2O_2-treated sample (A to C) or SSc cells (D); $^{\dagger\dagger}P < 0.01$ compared to UV-treated cells (E).

dependent on DDR and not ROS alone, we treated normal or A-T fibroblasts cells with bleomycin, which activates the DDR by creating DNA double-strand breaks (DSBs) and, incidentally, also induces fibrosis (*21*). Bleomycin repressed *WIF-1* and stimulated *COL1A1* expression in normal, but not in A-T, fibroblasts cells (Fig. 4, A and B, and fig. S6A); instead, *WIF-1* transcript abundance increased in the presence of bleomycin in A-T fibroblasts (Fig. 4A), further supporting a role for ATM in repressing *WIF-1* expression. We also knocked down ATM using targeted siRNA. Depletion of ATM in normal fibroblasts prevented WIF-1 silencing by bleomycin, whereas ATM knockdown increased WIF-1 abundance in SSc patient cells (fig. S6B).

The data thus far have suggested that ATM is a critical mediator of WIF-1 silencing in the presence of ROS and DNA damage. However, the question remained whether oxidative stress, in addition to DNA damage, was also involved in bleomycin-induced repression of WIF-1. Therefore, we assessed the abundance of ROS in normal fibroblasts using the ROS-sensitive fluorescent probe 2′,7′-dichlorfluorescein-diacetate (DCFH-DA) after treatment with bleomycin in the presence or absence of the various inhibitors. ROS were induced by bleomycin, but this induction was inhibited by the ATM inhibitor KU55933 or by the ROS inhibitor DPI (Fig. 4, C and D), suggesting that ATM promoted ROS abundance in normal fibroblasts after bleomycin. Furthermore, DPI or KU55933 prevented bleomycin-induced silencing of *WIF-1* and the induction of *COL1A1* expression (Fig. 4E). Finally, in SSc cells, DPI induced the expression of *WIF-1* and reduced that of *COL1A1* (fig. S7A), indicating that the conditions present in SSc fibroblasts are similar to those in normal fibroblasts exposed to oxidative stress or bleomycin. The data shown above suggest that ATM is both upstream (Fig. 4, C and D) and downstream (fig. S5) of ROS to inhibit *WIF-1* expression. However, these data do not clarify whether ATM induced by ROS is sufficient to silence *WIF-1* expression in the absence of classical DNA damage—DSBs—that selectively activates ATM (*22*). DSBs are recognized by ATM that phosphorylates γ-H2AX, the histone variant that specifically accumulates at DSBs. Cells exposed to a high concentration of H_2O_2 accumulate phosphorylated γ-H2AX, although less efficiently than bleomycin (fig. S7B), suggesting that ROS activate ATM both directly by oxidation (Fig. 3F) (*20*) and indirectly by inducing DSB.

The data thus far indicate that ROS and DNA damage silence WIF-1 and activate collagen. Therefore, we asked whether also other known profibrotic factors use the same mechanism(s). Specifically, we investigated whether transforming growth factor–β (TGF-β), which induces ROS and collagen

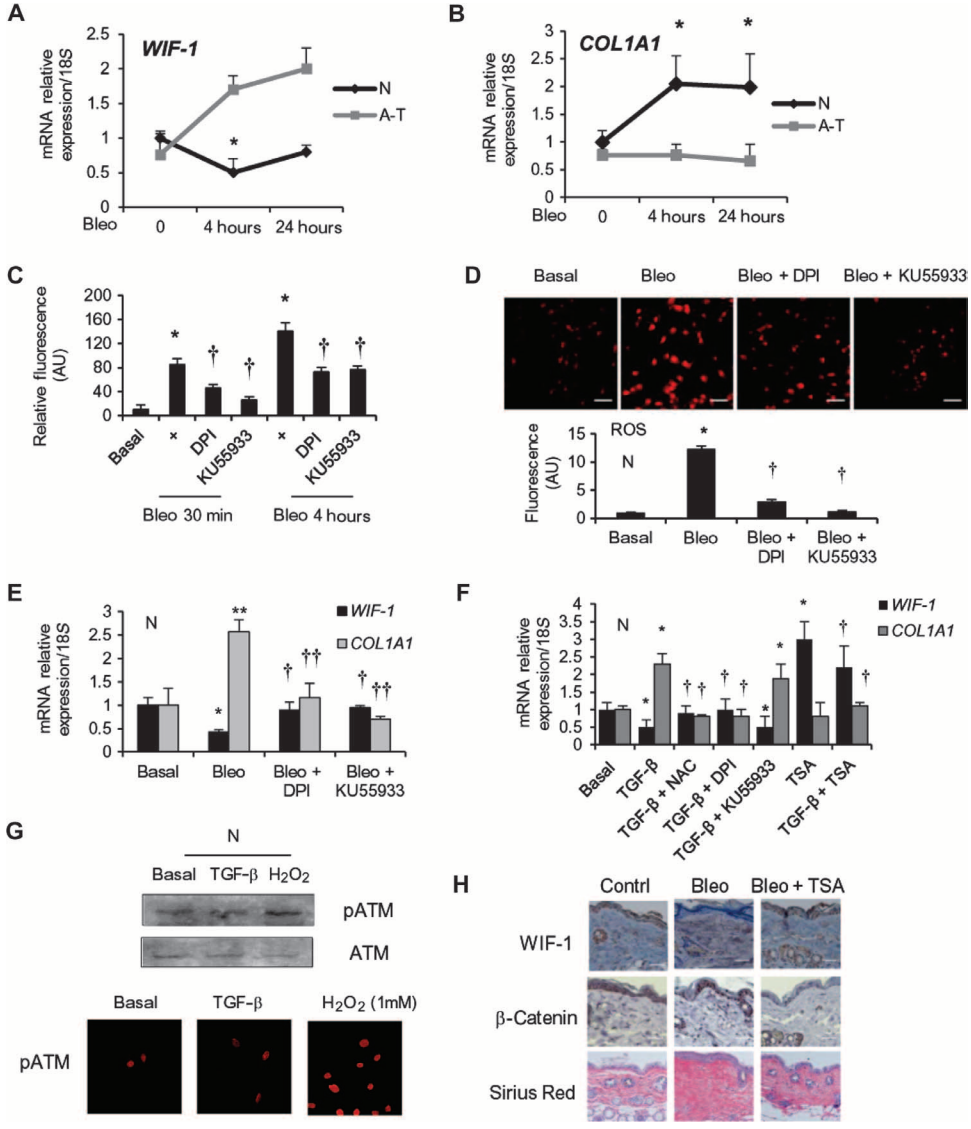

Fig. 4. ATM is essential for WIF-1 silencing by ROS and bleomycin. (A and B) *WIF-1* and *COL1A1* expression in serum-starved A-T or normal (N) fibroblasts during 24 hours of treatment with bleomycin (20 mU/ml). (C and D) Intracellular ROS after bleomycin (20 mU/ml) in normal fibroblasts pretreated with DPI or KU55933 (each 10 μM, 1 hour) assessed by fluorescence (C) and confocal microscopy (D). Images are representative of three experiments. (E) *WIF-1* and *COL1A1* expression in normal fibroblasts treated as in (C) and normalized to 18*S* RNA. (F) *WIF-1* and *COL1A1* mRNA abundance in normal fibroblasts pretreated with TSA (300 nM, 48 hours) or NAC, DPI, or KU55933 (each 10 μM, 1 hour) followed by TGF-β (10 ng/ml, 24 hours). Data in (A) to (F) are means ± SD of three independent experiments. (A, B, and F) $^{*}P < 0.01$ against basal, $^{\dagger}P < 0.05$ against TGF-β–treated samples; (C to E) $^{*}P < 0.05$ and $^{**}P < 0.01$ against basal, $^{\dagger}P < 0.05$ and $^{\dagger\dagger}P < 0.01$ against bleomycin-treated samples. (G) Immunoblot and confocal microscopy for phosphorylated ATM in fibroblasts treated with H_2O_2 (1 mM, 2 hours) or TGF-β (10 ng/ml, 24 hours). Blots and images are representative of three experiments. (H) Immunohistochemistry for WIF-1 and β-catenin in skin from mice subcutaneously injected with either phosphate-buffered saline (PBS) (Contrl) or bleomycin (Bleo) compared with mice that received intraperitoneal injection of TSA before bleomycin injection (Bleo + TSA). Images are representative of six mice each. Scale bars, 100 μm (D and H).

(*23*), had a suppressive effect on *WIF-1* expression, and whether it acted through ATM. Normal fibroblasts were preexposed to one of several inhibitors [*N*-acetyl cysteine (NAC) or DPI to reduce ROS, KU55933 to inhibit ATM, or TSA to inhibit HDAC] and treated with TGF-β for 24 hours. TGF-β reduced *WIF-1* expression in a ROS- and HDAC-dependent but ATM-independent manner, because NAC and DPI, and TSA prevented the effects of TGF-β on *COL1A1* and *WIF-1* expression, whereas KU55933 did not (Fig. 4F). TGF-β, under these conditions, did not activate ATM (Fig. 4G), suggesting that TGF-β–induced ROS can activate HDAC (*24*–*26*) and repress *WIF-1*, but do not induce DNA damage and ATM. Moreover, these data show that the effects of ATM and ROS on *WIF-1* silencing can be dissociated and suggest that ROS induced by TGF-β are neither persistent nor high enough to induce ATM.

Because inhibition of HDAC by TSA or of ATM by KU55933 individually increased *WIF-1* expression in SSc cells (Figs. 1F and 3D), we investigated whether TSA and KU55933 inhibit the same signaling pathway. The effects of TSA and KU55933 on *WIF-1* and *COL1A1* expression in SSc cells were not additive (fig. S8), suggesting that their targets, HDAC and ATM, are in the same pathway.

To test the in vivo relevance of *WIF-1* silencing, and the role of HDAC therein, we investigated its expression in a standard model of fibrosis induced by bleomycin (*27*). Briefly, repeated subcutaneous injections of bleomycin for 24 to 28 days were used to induce fibrosis in mice, confirmed by α-SMA (α–smooth muscle actin) abundance and Masson's trichrome staining (fig. S9). In subgroups of bleomycin-treated mice, pretreatment with intraperitoneal injections of TSA for 4 weeks prevented the decreased WIF-1 and increased β-catenin abundance observed after bleomycin exposure (Fig. 4H), suggesting that bleomycin-induced Wnt signaling was mediated by an HDAC-dependent mechanism in vivo. Whether ATM mediates this pathway in vivo as well remains to be investigated.

Transcription factors c-Jun and activating transcription factor 3 silence WIF-1

To identify the transcription factor (or factors) responsible for WIF-1 silencing induced by ROS and DNA damage, we used a combination of genetic and biochemical approaches to examine transcription factors induced by stress or DNA damage. In primary human fibroblasts, inhibition of nuclear factor κB (NF-κB), by expressing the dominant-inhibitor mutant form of the NF-κB inhibitor IκBα (IκBαM) (fig. S10A) (*28*), did not prevent the repression of *WIF-1* in response to H_2O_2 (fig. S10B), although it did inhibit that of NF-κB targets *IL6* and *CXCL1* in response to tumor necrosis factor, an activator of NF-κB (fig. S10C). Similarly, NF-κB inhibition did not affect *WIF-1* expression in SSc fibroblasts (fig. S10D), indicating that activation of NF-κB did not mediate transcriptional repression of WIF-1.

We then turned our attention to members of the AP1 family and inhibited several of these in SSc cells by expressing one of several dominant-negative AP1 constructs [TAM67, derived from c-Jun (*29*), or a-Fos derived from c-Fos, the human homolog of the retroviral oncogene v-Fos (*29*)] or the wild-type Fos-related antigen 1 (FRA1) to titrate possible AP1-linked repressors (*30*). Among the two dominant-negative mutants or wild-type FRA, only TAM increased *WIF-1* expression (Fig. 5A), suggesting that c-Jun inhibits *WIF-1* expression. Confirming this hypothesis, partial depletion of c-Jun with siRNA (fig. S11A) increased *WIF-1* expression but did not significantly modify *COL1A1* expression in SSc cells (Fig. 5B), suggesting that c-Jun was necessary for *WIF-1* repression, but perhaps not for induction of *COL1A1* expression. To find the missing factor regulating *COL1A1* expression, we investigated the abundance of various transcription factors that interact with c-Jun. We found that the abundance of activating transcription factor 3 (ATF3), a cAMP (adenosine 3′,5′-monophosphate)–responsive element binding (CREB) protein–like stress transcription factor (*31*), was greater in SSc cells than in normal fibroblasts (Fig. 5C and fig. S11B). In SSc cells, partial siRNA-mediated knockdown of ATF3 (fig. S11C) induced the expression of *WIF-1* and reduced that of *COL1A1* (Fig. 5D), suggesting that, whereas both c-Jun and ATF3 can silence *WIF-1* in SSc cells, only ATF3 can induce *COL1A1* expression. In normal fibroblasts, ATF3 and c-Jun were each also involved in the bleomycin-induced

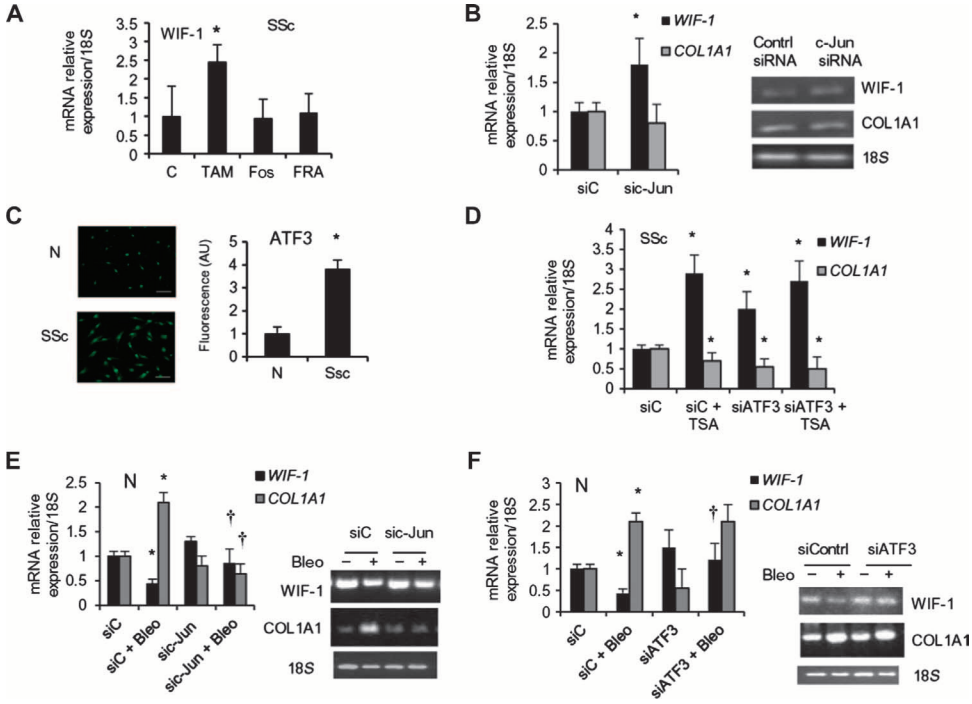

Fig. 5. The AP1 family member c-Jun and the stress-induced transcription factor ATF3 silence *WIF-1* and induce *COL1A1*. (**A**) *WIF-1* mRNA in SSc fibroblasts transfected with the control (C) or an AP1 family construct-encoding plasmid. (**B**) RT-PCR (left) or semiquantitative PCR (right) for *WIF-1* and *COL1A1* mRNA in SSc fibroblasts transfected with c-Jun siRNA (sic-Jun) or control siRNA (siC) for 48 hours. (**C**) Confocal microscopy for ATF3 in normal (N) or SSc fibroblasts. Scale bars, 100 μm. One hundred cells per field were scored. (**D**) *WIF-1* and *COL1A1* mRNA abundance in SSc fibroblasts transfected with ATF3 siRNA (siATF3) or control siRNA (siC) for 48 hours, and then treated with TSA (300 nM) for 24 hours, then lysed. (**E** and **F**) RT-PCR (left) or semiquantitative PCR (right) for *WIF-1* and *COL1A1* mRNA expression in normal fibroblasts transfected with control siRNA or siRNA against c-Jun (E) or ATF3 (F) for 48 hours and then treated with bleomycin (20 mU/ml) for 4 hours. Data in (A) to (F) are means ± SD from three independent experiments. $^{*}P < 0.05$ against basal or control, $^{\dagger}P < 0.05$ compared to bleomycin-treated cells.

repression of WIF-1; however, only c-Jun appeared to be involved in bleomycin-induced induction of *COL1A1* (Fig. 5, E and F). The different regulation of *COL1A1* in normal and SSc cells may be dependent on the abundance of other members of the AP1 family in SSc patient cells (*32*, *33*), but this is speculation and requires further investigation.

To dissect the roles of c-Jun and ATF3 on *WIF-1* expression, we monitored the recruitment of these two factors and a class I HDAC (HDAC3) to the promoter of *WIF-1*. In normal and SSc fibroblasts, ATF3, c-Jun, and HDAC3 each immunoprecipitated with the promoter of *WIF-1*, and the abundance of ATF3 and HDAC3 present on the promoter was increased in SSc patient cells (fig. S12, A to C). In SSc patient cells, partial knockdown of c-Jun with siRNA (figs. S11A and S13A) reduced the amount of ATF3 and HDAC3 that were bound to the *WIF-1* promoter (fig. S13, B and C). Partially silencing ATF3 (figs. S11C and S13D) also reduced the abundance of c-Jun that was bound to the *WIF-1* promoter (fig. S13E), whereas ATF3 knockdown had no significant effect on the recruitment of HDAC3 (fig. S13F). Together, the data suggest that although the amount of c-Jun that bound to *WIF-1* promoter in SSc and normal cells was similar (fig. S12B), recruitment of c-Jun and ATF3 to the *WIF-1* promoter in SSc cells was at least partially reciprocally dependent. We speculate that reciprocal stabilization of a complex between c-Jun and ATF3 (c-Jun/ATF3 complex) and c-Jun–mediated targeting of HDAC3 to the *WIF-1* promoter are responsible for WIF-1 silencing.

ATM activates ATF3 and c-Jun transcription factors

So far, the data indicate that ATM mediates the repression of WIF-1 after ROS or DNA damage, and that c-Jun and ATF3 have a role in silencing *WIF-1* expression in SSc patient cells. To investigate the link between ATM and the c-Jun/ATF3 complex, we analyzed this mechanism in response to DNA-damaging agents in normal cells compared with fibroblasts from ataxia telangiectasia (AT) patients, which are deficient for wild-type ATM. Unlike that in normal fibroblasts, ATF3 abundance was not induced by H_2O_2 in A-T fibroblasts (GM05823) (Fig. 6A). Because A-T fibroblasts additionally had not shown WIF-1 repression in response to H_2O_2 (Fig. 3F) or bleomycin (Fig. 4A), and we had inferred that ATF3 mediated the repression of WIF-1 in bleomycin-treated cells (Fig. 5F), we suggest that the transcriptional repression of *WIF-1* after DNA damage occurs in an ATM-dependent manner in normal fibroblasts.

Therefore, we examined the role of ATM in WIF-1 repression further by examining possible mediators between ATM and the c-Jun or ATF3 transcription factors. The phosphorylation of c-Jun at Ser^{73} and Thr^{91} by c-Jun N-terminal kinases 1 and 2 (JNK1/2) (*34*, *35*) was less in AT fibroblasts in response to H_2O_2 than in normal fibroblasts (fig. S14), suggesting that JNK may have a role downstream of ATM in repressing *WIF-1* expression. SSc cells had increased JNK-phosphorylated c-Jun, comparable to those induced by bleomycin in normal fibroblasts (Fig. 6B). Another site at the N terminus of c-Jun (Thr^{95}) is phosphorylated in stressed cells (*36*), and when mutated to a nonphosphorylatable residue (T95A) reduces JNK-mediated phosphorylation of c-Jun at Ser^{91} (*35*). In SSc cells, which also had increased ATF3 (Fig. 5C and fig. S11B), expression of the T95A c-Jun mutant induced *WIF-1* but suppressed *COL1A1* expression (Fig. 6C). In contrast, the phosphomimetic mutant c-Jun, T95D, did not significantly alter either WIF-1 or COL1A1 expression (Fig. 6C), possibly because the SSc cells are already saturated with ATM-phosphorylated c-Jun. We hypothesize that T95A c-Jun titrates the endogenous phosphorylated protein in heterodimers (with AP1 or ATF3). Conversely, in normal fibroblasts (in which c-Jun was not ATM-phosphorylated), the expression of the phosphomimetic c-Jun mutant T95D suppressed *WIF-1* and stimulated *COL1A1* expression, whereas the nonphosphorylatable mutant T95A had no significant effect (Fig. 6D). In normal fibroblasts, the phosphomimetic mutant T95D induced *ATF3* expression even in the presence of T95A because ATM-mediated phosphorylation is not active, suggesting that c-Jun phosphorylation is essential for *ATF3* induction (Fig. 6E).

To investigate whether ATM might be the kinase that phosphorylates the Thr^{95} site in c-Jun, HeLa cells (a cancer cell line of epithelial origin and amenable to transfection) and human fibroblasts were transfected with hemagglutinin (HA)–tagged wild-type or mutant c-Jun and treated with bleomycin to activate the pathway thus far investigated. In cell lysates, immunoprecipitation for the HA tag was performed followed by Western blotting with an antibody that detects phosphorylated Ser/Thr ATM/ATR substrates. Only wild-type c-Jun was detected by the antibody in HeLa

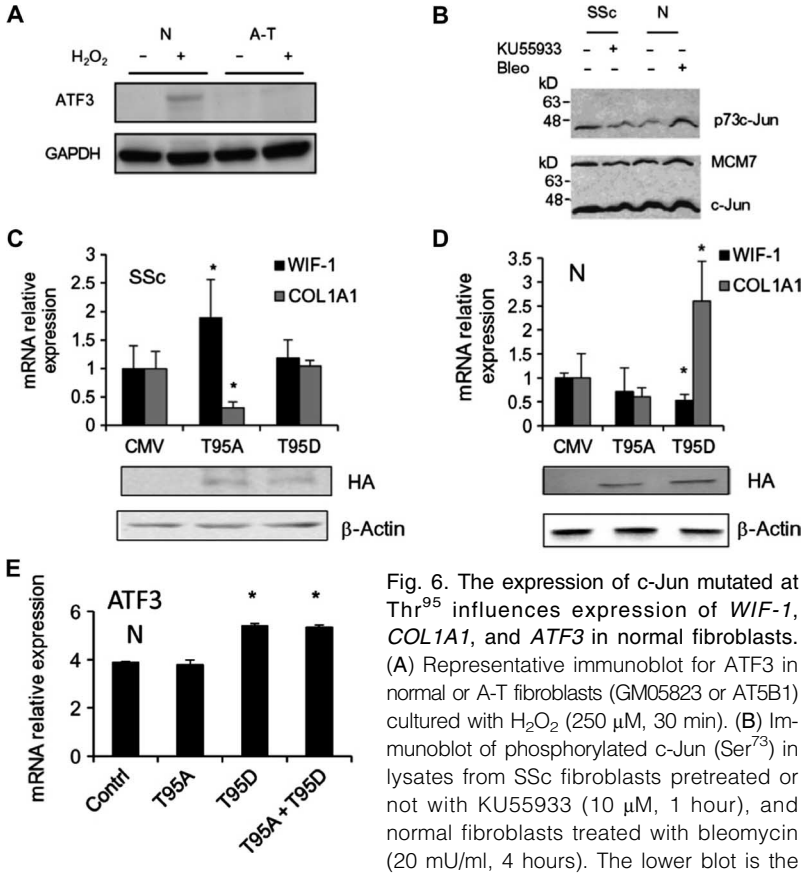

Fig. 6. The expression of c-Jun mutated at Thr^{95} influences expression of *WIF-1*, *COL1A1*, and *ATF3* in normal fibroblasts. (**A**) Representative immunoblot for ATF3 in normal or A-T fibroblasts (GM05823 or AT5B1) cultured with H_2O_2 (250 μM, 30 min). (**B**) Immunoblot of phosphorylated c-Jun (Ser^{73}) in lysates from SSc fibroblasts pretreated or not with KU55933 (10 μM, 1 hour), and normal fibroblasts treated with bleomycin (20 mU/ml, 4 hours). The lower blot is the upper gel reblotted for c-Jun and mini chromosome maintenance protein MCM7 (loading control). (**C** and **D**) RT-PCR analysis for *WIF-1* and *COL1A1* in SSc (C) and normal (D) fibroblasts transfected with empty vector [cytomegalovirus (CMV)] or vector encoding either wild-type or mutant HA-tagged c-Jun (T95A or T95D). Blots for HA below graphs confirm transfection. (**E**) RT-PCR analysis for ATF3 in normal fibroblasts transfected with T95D or T95A c-Jun–HA fusions. Blots are representative, and data in (C) to (E) are means ± SD of three independent experiments. **P* < 0.05 compared to empty vector.

cells and fibroblasts (fig. S15, A and C). Endogenous c-Jun in HeLa cells (fig. S15B) or in normal fibroblasts (fig. S15D) exposed to bleomycin was recognized by this ATM substrate antibody, and the signal was inhibited by pharmacological inhibition (fig. S15, B and D) or siRNA-mediated knockdown of ATM (fig. S15E). These data suggest that ATM phosphorylates c-Jun at Thr^{95}. This may facilitate JNK-dependent phosphorylation of c-Jun (fig. S14) and the induction and recruitment of ATF3 (Fig. 6E) and HDAC3 (fig. S13C), and ultimately represses *WIF-1* expression, enabling Wnt signaling.

DISCUSSION

We showed that *WIF-1* expression is decreased in SSc cells through deacetylation induced by oxidative DNA damage, leading to increased Wnt signaling, associated with fibrosis. The suppression of *WIF-1* expression by oxidative DNA damage and ATM is unique among the Wnt inhibitors, and the indirect activation of ATF3 by ATM ties this mechanism to an extensive network of stress-inducible transcription factors (*37*). A schematic diagram illustrating the various components involved in WIF-1 silencing and COL1A1 induction in normal and SSc patient fibroblasts is shown in Fig. 7.

WIF-1 is a ROS marker

Our findings indicate that WIF-1 is a marker of oxidative DNA damage because ROS induced by short pulses of PDGF or low concentrations of H_2O_2 activated its expression, whereas higher ROS exposure silenced it. β-Catenin abundance asymmetrically followed WIF-1 suppression: low WIF-1 expression correlated with high total and nuclear β-catenin accumulation, leading to increased Wnt signaling, as seen in colon cells (*38*) or in mouse ectoderm (*39*). ROS can activate ATM directly (*20*, *40*) or through DNA damage (*22*), but we also propose that ROS are induced by the activity of ATM because inhibition of ATM reduced ROS. ATM seems to be a regulator of cellular ROS, and it may finely tune ROS content in stressed cells (*41*, *42*). When DNA is damaged, ATM induces ROS and transiently renders the cell refractory to exogenous signals. This ROS-adaptive response to stress is conserved in *Saccharomyces cerevisiae* (*43*), and we speculate that high levels of ROS during repair provide selection for increased fitness of stressed cells.

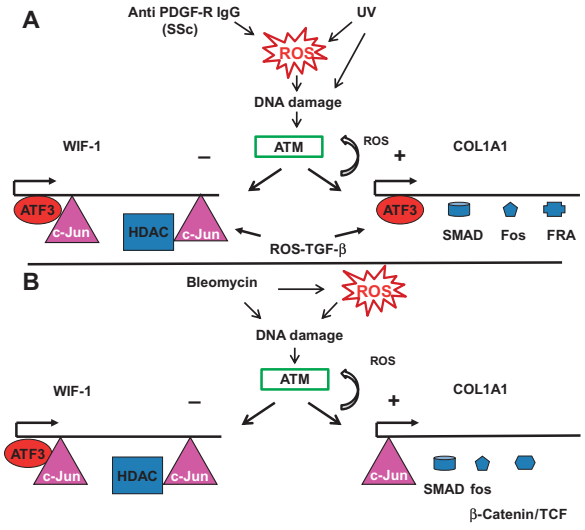

Fig. 7. Control of WIF-1 expression by stress and DNA damage. Schematic illustrating the series of events leading to WIF-1 silencing and collagen induction in SSc and normal cells. (**A**) In SSc, *COL1A1* can be induced by several members of the AP1 family (but not c-Jun), TGF-β signaling (through SMAD), and by ATF3. DNA damage or ROS activate ATM and JNK. ATM phosphorylates c-Jun and facilitates the phosphorylation of c-Jun by JNK. Phosphorylated c-Jun activates ATF3. c-Jun, ATF3, and HDAC3 bind the *WIF-1* promoter and repress its transcription. (**B**) In normal fibroblasts, bleomycin induces DNA damage, which activates ATM and ROS, which in turn activate c-Jun, JNK, and ATF3. As in SSc cells, ATF3, c-Jun, and HDAC3 are recruited to the *WIF-1* promoter and silence the gene. Unlike in SSc cells, however, c-Jun, in combination with other AP1 family members (for example, c-Fos), induces β-catenin/TCF–dependent Wnt signaling and *COL1A1* expression.

ATM is critical to the suppression of WIF-1

The transcription of *WIF-1* was regulated by ATF3 and c-Jun. ATF3 is a member of the CREB family and is induced by a variety of stress signals, including DNA damage (*31*). c-Jun is a member of the AP1 family of transcription factors and, by associating with various proteins, regulates the expression of genes involved in the cellular stress response (*44*, *45*). In our study, ATF3 was induced in normal cells only when ATM was functional, explaining why ATM-defective cells were unable to respond to bleomycin. In SSc cells, persistent oxidative stress (*10*) and DNA damage maintain a high abundance of ATF3 and phosphorylated c-Jun, which are recruited to the *WIF-1* promoter and silence the gene, resulting in increased Wnt signaling (*9*). Our data also suggest that ATM amplifies the efficacy of JNK-mediated phosphorylation of c-Jun, revealing a possible explanation for why ATM-defective livers show reduced phosphorylated c-Jun (*46*). In our study, under conditions of DNA damage, ROS-adaptive response induced by ATM stimulates JNK, c-Jun, and, eventually, ATF3 expression (*47*). Thus, ATF3 and phosphorylated c-Jun enhance Wnt signaling perhaps by two mechanisms: by reducing WIF-1–mediated inhibition of soluble Wnt, and by cooperating with β-catenin to induce transcription (*48*).

The mechanism of *WIF-1* silencing has implications for cancer and fibrosis

WIF-1 silencing is a selected phenotype both in stressed mesenchymal cells and in epithelial neoplastic cells. *WIF-1* is one of the most frequent silenced genes in cancer, and its loss is common in many tumors (*14*, *49*). Targeted disruption of WIF-1 accelerates osteosarcomagenesis, without interfering with normal bone development in mice (*50*). Our data suggest that persistent oxidative DNA damage initially silences WIF-1 by histone deacetylation in fibroblasts and possibly other cell types, whereas WIF-1 is silenced predominantly by methylation in epithelial cells (*14*). We speculate that in fibroblasts, robust stimulation of histone acetylation can reactivate the expression of the gene and repress Wnt signaling, whereas in epithelial cells, WIF-1 silencing may be permanent, irreversible, and positively selected during neoplastic progression (*49*, *51*).

If WIF-1 silencing occurs in mesenchymal cells, Wnt signaling leads to senescence and exit from the cycle (*52*); differentiated myofibroblasts (*6*) or myoblasts (*8*) exit from the cycle, synthesize collagen or α-SMA, and accumulate ROS and β-catenin, which are the hallmarks of fibrosis and wound healing (*9*, *10*, *52*, *53*). PDGF or TGF-β and other soluble factors (such as the IgG of SSc patients) cooperate efficiently with β-catenin to activate a transcription program leading to fibrosis and senescence (*54*). We propose that WIF-1 silencing is accomplished by two ROS signaling cascades: (i) low or transient ROS (TGF-β) activate HDAC (*22*–*24*), but not ATM; (ii) high or persistent ROS induce DNA damage and ATM. From this perspective, fibrosis represents an amplified secretory response of senescent fibroblasts to DNA damage associated with wound healing

(*55*). We speculate that loss of secreted WIF-1 amplifies local Wnt action and induces a proliferative burst of surrounding epithelial cells and terminal differentiation of fibroblasts. Only cells that have efficiently repaired the DNA respond to Wnt because damaged cells succumb to apoptosis through clashing signals of arrest and stimulation of growth. This provides a robust selection for fitness of epithelial cells surrounding damaged and senescent fibroblasts. Our findings in a breast cancer epithelial cell line suggests that methylation of the *WIF-1* promoter might reinforce local Wnt signaling in epithelial cells (*56*). This finding provides a mechanism linking ROS, DNA damage, fibrosis, and cancer (*57*) and may explain the higher incidence of lung cancer in SSc patients (*58*).

In conclusion, our findings exploring activated Wnt signaling in fibrosis or during neoplastic progression indicate that DNA damage and genome stability checkpoints link ROS, Wnt, and fibrosis, thus integrating many apparently heterogeneous phenotypes associated with fibrosis and cancer.

MATERIALS AND METHODS

Antibody purification

IgGs were purified from the serum of normal and SSc human subjects, after oral and written informed consent, using gravity flow columns packed with Protein A/G–agarose following the manufacturer's instructions (Pierce). The eluted IgG fractions were subjected to buffer exchange with PBS using desalting columns (limit of 5 kD) (Pierce). Purity of IgG preparations was confirmed by immunoblotting with specific cytokine antibodies [PDGF, TGF-β, and IL-1 to IL-6 (interleukin-1 to -6)]. For the recombinant antibody VH PAM-Vk16F4, the VH and VL sequences were cloned from the cDNA (complementary DNA) of peripheral lymphocytes of an SSc patient. Sequence analysis identified the VH and VL sequences, which were inserted into the Xba I–Sac I and Hind III–Eco RI restriction sites, respectively, under the control of the human cytomegalovirus (HCMV) promoter in the plasmid vector pDR12, which contains an ampicillin resistance gene for selective amplification (fig. S16). The plasmid was amplified in *E. coli* and transfected into Chinese hamster ovary cells, and the IgG was purified by immunoaffinity. The study was approved by the institutional ethics committee at the Università Politecnica delle Marche.

Cells and treatments

Human skin fibroblasts were obtained from punch biopsies taken from the forearms of normal volunteers and from the skin of patients who fulfilled the preliminary criteria of the American Rheumatism Association for the diagnosis of SSc, as described previously (*42*). Mouse embryo fibroblasts (MEFs) derived from PDGF receptor knockout embryos that do not express α and β chains of PDGFR subunits (F–/– cells) infected with PDGFR α subunit (Fα cells) were previously described (*11*). Fibroblasts, HeLa cells, and MEFs were grown in Dulbecco's modified Eagle's medium (DMEM), containing glucose (1 g/liter), supplemented with 10% fetal bovine serum (FBS), penicillin (100 U/ml), and streptomycin (100 g/ml) (Gibco). Human control (GM00024) and A-T fibroblasts (GM05823 also known as AT5B1) were obtained from Coriell Institute and maintained in EMEM (Eagle's minimum essential medium) supplemented with 15% FBS, penicillin/streptomycin (100 mU/ml), and 2 mM glutamine (Gibco). For PDGF treatments, subconfluent fibroblasts were treated with IgG (0.2 μg/μl) or recombinant PDGF-BB (15 ng/ml) (Sigma) after 4 hours of starvation (0.2% FBS) for 24 hours. In selected experiments, cells were incubated with 300 nM TSA (Sigma) for 48 hours, 4 μM 5-aza-2′-deoxycytidine (5-azacytidine; Sigma) for 24 hours, cisplatinum (5 μM; Sigma) for 24 hours, 10 μM DPI (Calbiochem) for 1 hour, KU55933 (Calbiochem) for 1 hour, and bleomycin (20 mU/ml; Sigma) for 4 or 24 hours, as indicated in the relevant legend. For UV experiments, cells were pretreated with 10 μM KU55933for 1 hour and then irradiated with UV (80 J/m^2) and incubated for a further 1 or 2 hours. Cells were transiently transfected with siRNA against *c-JUN* (Santa Cruz), *ATF-3* (Qiagen), *ATM* (Qiagen), or *WIF-1* (Santa Cruz), or transfected with the dominant-negative AP1 constructs c-Jun–derived GFP (green fluorescent protein)–TAM67 and c-Fos–derived GFP–a-Fos plasmids (*26*), or the T95A or T95D c-Jun mutant (*32*) using Lipofectamine 2000 reagent (Life Technologies) following the manufacturer's instructions. Cells were processed 48 hours after transfection, except the WIF-1 siRNA-transfected cells, which were lysed 72 hours after the transfection.

Western blotting analysis

Total cell lysates were obtained in radioimmunoprecipitation assay (RIPA) buffer (2.5 mM Na-pyrophosphate, 1 mM β-glycerophosphate, 1 mM $NaVO_4$, 1 mM NaF; Sigma) supplemented with a cocktail of protease inhibitors. The samples were stored for 30 min at 4°C and centrifuged at 10,000 rpm for 10 min at 4°C. Samples were resolved on a 4 to 12% gradient SDS–polyacrylamide gel electrophoresis (SDS-PAGE) and transferred onto a nitrocellulose membrane (Life Technologies). After blocking with 0.5% Tween for 1 hour, immunoblots were incubated with antibodies against WIF-1 (1:1000; Abcam), β-catenin (1:1000; Abcam), pATM (1:500; Abcam,), ATM (1: 500; Novus Biologicals), 53BP1 (1:500; Novus Biologicals), β-actin (1:1000; Santa Cruz Biotechnology), phospho-(Ser/Thr) ATM/ATR substrate antibody (1:1000, Cell Signaling Technology), HA (1:500; Covance), Ser^{73} c-Jun (1:1000; Cell Signaling Technology), and Thr^{91} c-Jun (1:1000; Cell Signaling Technology) overnight at 4°C. After incubation with horseradish peroxidase (HRP)–conjugated antibodies against rabbit or mouse IgG (Santa Cruz Biotechnology) for 1 hour, signals were detected with ECL Western Blotting Detection Reagents (Amersham Bioscience).

ROS detection

Fluorimetric determination of intracellular ROS was carried out using DCFH-DA (Life Technologies), as previously described (*9*), using a multiwell plate reader (Wallac 1420, PerkinElmer). For confocal microscopy experiments, cells were seeded on coverlids, loaded with 10 μM DCFH-DA or 10 μM DHE (Life Technologies) for 30 min, washed with PBS, and then visualized on a confocal microscope Eclipse C1 (Nikon).

Quantitative real-time PCR analysis

Total RNA isolation from normal, scleroderma, and *ATM*$^{-/-}$ fibroblasts was isolated with PureLink RNA Mini Kit (Life Technologies) according to the manufacturer's instructions. Total RNA (1 g) of each sample was reverse-transcribed with the iScript cDNA Synthesis Kit (Bio-Rad) according to the manufacturer's instructions. Quantitative RT-PCR was performed with SYBR Green PCR Master Mix (Bio-Rad). Primers sequences for amplification are represented in table S1. The amplification was carried out through 45 cycles of 95°C for 15 s and 60°C for 1 min in a iCycler iQ Real-Time PCR Detection System (Bio-Rad). Relative expression was calculated with the $2^{-\Delta\Delta Ct}$ method.

Methylation analysis using bisulphite genomic sequencing

The promoter region and the entire coding sequence of human *WIF-1* gene were analyzed for CG content. A CpG island was determined on the basis of a 200–base pair (bp) length of DNA with a CG content greater than 50% and a CpG/GpC ratio greater than 0.5 using CpG plot program (http://www.ebi.ac.uk/emboss/cpgplot/). Bisulphite genomic sequencing was used to analyze the methylation patterns of individual DNA molecules. Sodium

bisulphite conversion of genomic DNA (about 2 μg for each conversion) was obtained using EpiTect Bisulfite Kit (Qiagen) following the purchaser's instructions. Amplicons used for methylation analysis were obtained from about 50 ng of bisulphite threaded genomic DNA. Specific primers used for these PCRs were as follows: WifBS-Fw1: –409 –390 5′-GAGTGATGTTTTAGGGGTTT-3′, WifBS-Rv1: –16 +5 5′-CCTAAATACCAAAAAACCTAC-3′, WifBS-Fw2: 16 +5 5′-GTAGGTTTTTTGGTATTTAGG-3′, WifBS-Rv2: +242 +263 5′-TCCATAAATACAAACTCTCCTC-3′. Amplifications were carried out on 10 ng of bisulphite-treated DNA using HotStarTaq DNA Polymerase (Qiagen) for 15 min at 95°C, followed by 50 cycles of 30 s at 95°C, 40 s at 53°C, and 1 min at 72°C, then a final elongation of 10 min at 72°C before holding at 4°C in a final reaction volume of 50 μl. Confirmation of PCR product quality and freedom from contamination was established on 2% agarose gels with ethidium bromide staining. PCR products were cloned into the pGEM-T Easy Vector provided by Promega pGEM-T Easy Vector System II, following the manufacturer's procedures. Positive-screened colonies contained the unique sequence of one individual DNA molecule. Plasmid DNA from the selected positive colonies containing vectors with the insert was purified using the Qiagen Plasmid Mini Kit. Purified plasmids were sequenced in both directions using T7 and Sp6 primers. Twenty independent clones for each genomic preparation and fragment of interest were sequenced to determine the methylation pattern of individual molecules. Sequencing was performed at the CEINGE Sequencing Core Facility, Naples, Italy.

Bleomycin-induced dermal fibrosis

Skin fibrosis was induced in 6- to 8-week-old C3H/HeJ mice by subcutaneous injection in defined areas of the upper back of bleomycin for 24 to 28 days as described (*27*).

Histological analysis

Skin sections were fixed in 4% formalin and embedded in paraffin. Sections (5 μm) were stained with Sirius Red for the analysis of connective tissue, and dermal thickness was analyzed by measuring the distance between the epidermal-dermal junction and the dermal–subcutaneous fat junction at sites of induration in three consecutive skin sections from each animal. In each series of experiments, the dermal thickness was calculated as the fold increase compared with the dermal thickness in controls.

Immunohistochemistry

Skin sections were deparaffinized, rehydrated, and stained with WIF-1 and β-catenin antibodies (1:100; Abcam) overnight at 4°C, washed, and incubated with biotinylated mouse IgG antibody for 1 hour at room temperature. The peroxidase ABC method was performed for 1 hour using diaminobenzidine hydrochloride (DAB) as chromogen.

Immunofluorescence

Cells were fixed for 5 min with 4% paraformaldehyde, permeabilized with 0.2% Triton X-100, and incubated with the following primary antibodies overnight at 4°C: WIF-1 (1:100; Abcam), β-catenin (1:100; Abcam,), pATM (1:100; Abcam), and type 1 collagen (1:200; Millipore). Cells were then washed and labeled with Alexa 488– or Alexa 546–conjugated antibodies (Life Technologies) and counterstained with SYTOX Green, a DNA counterstain for fixed cells (Life Technologies). Controls were incubated with secondary antibodies alone. Cells were analyzed using the confocal microscope Eclipse C1 (Nikon).

Chromatin immunoprecipitation

Cells (1×10^6) were fixed by adding formaldehyde directly to culture medium to a final concentration of 1% for 10 min at room temperature and washed twice using ice-cold PBS containing 1× protease inhibitor cocktail (Roche Applied Science) and 1 mM PMSF (phenylmethylsulfonyl fluoride). Fixed cells were harvested, and the pellet was resuspended in 200 μl of SDS lysis buffer [Chromatin Immunoprecipitation (ChIP) Assay Kit, Upstate]. After 10 min of incubation on ice, the lysates were sonicated to shear DNA to 300- and 1000-bp fragments. Sonicated samples were centrifuged and supernatants were diluted 10-fold in the ChIP dilution buffer (ChIP Assay Kit, Upstate). An aliquot (1:50) of sheared chromatin was further treated with proteinase K, phenol/chloroform-extracted, and precipitated to determine DNA concentration and shearing efficiency (input DNA). The ChIP reaction was set up according to the manufacturer's instructions. Briefly, the sheared chromatin was precleared for 2 hours with 20 μl of Protein A– or Protein G–agarose (Upstate) and 2 μg of nonimmune IgG (Santa Cruz Biotechnology), and then was divided into two aliquots and incubated at 4°C for 16 hours with 20 μl of Protein A/G–agarose and 2 μg of the specific antibody ATF3 (Santa Cruz Biotechnology), HDAC3 (Santa Cruz Biotechnology), c-Jun (Santa Cruz Biotechnology), and nonimmune IgG, respectively. Agarose beads were washed with wash buffers according to the manufacturer's instructions, and immunoprecipitated DNA was recovered and subjected to quantitative PCR using the primers indicated in the legend of the specific figures and in table S1. Primers for *WIF-1* ChIP were (forward) 5′-CGGGTTATCAGGGAGACAGA-3′ and (reverse) 5′-CTCCCTTTCAGCCAGTAGGA-3′.

Ethical statement

Use of human material was approved by the Institutional Ethical Committee of Università Politecnica delle Marche, Ancona, Italy, and consent was obtained from all subjects who participated in this study. All assays were performed in blind fashion on coded samples.

Statistics

Data were quantified as means ± SD and were analyzed with the nonparametric Mann-Whitney test. Data were analyzed using Prism 4 (GraphPad Software Inc.). *P* values less than 0.05 were considered significant.

SUPPLEMENTARY MATERIALS

www.sciencesignaling.org/cgi/content/full/7/341/ra84/DC1

Fig. S1. *WIF-1* is methylated in MCF7 breast cancer cells, not in normal or SSc fibroblasts.
Fig. S2. *WIF-1* silencing induces β-catenin abundance.
Fig. S3. The oxidase inhibitor DPI inhibits ROS accumulation in SSc cells.
Fig. S4. Among Wnt inhibitors, only *WIF-1* is silenced by ATM.
Fig. S5. ATM mediates H_2O_2-induced silencing of *WIF-1*.
Fig. S6. Loss of ATM restores WIF-1 abundance in SSc fibroblasts and inhibits bleomycin-induced silencing of *WIF-1*.
Fig. S7. Inhibition of ROS production in SSc cells increases *WIF-1* expression and inhibits expression of the gene encoding collagen.
Fig. S8. The effects of HDAC and ATM inhibitors on *WIF-1* expression are not additive.
Fig. S9. Bleomycin-induced skin fibrosis is inhibited by an HDAC inhibitor, TSA.
Fig. S10. NF-κB does not mediate *WIF-1* silencing induced by ROS.
Fig. S11. Efficiency of c-Jun and ATF3 knockdown.
Fig. S12. ATF3, c-Jun, and HDAC3 are recruited to the *WIF-1* promoter in SSc cells.
Fig. S13. The recruitment of c-Jun to the *WIF-1* promoter in SSc cells is partially dependent on ATF3.
Fig. S14. Phosphorylation of c-Jun is induced by H_2O_2 in wild-type, but not in A-T, cells.
Fig. S15. c-Jun is a substrate of ATM in HeLa cells and human fibroblasts exposed to bleomycin.
Fig. S16. pDR12 plasmid construct.
Table S1. List of primers.

REFERENCES AND NOTES

1. J. C. Gross, V. Chaudhary, K. Bartscherer, M. Boutros, Active Wnt proteins are secreted on exosomes. *Nat. Cell Biol.* **10**, 1036–1045 (2012).
2. L. Ling, V. Nurcomb, S. M. Cool, Wnt signaling controls the fate of mesenchymal stem cells. *Gene* **433**, 1–7 (2009).

3. C. M. Cruciat, C. Niehrs, Secreted and transmembrane Wnt inhibitors and activators. *Cold Spring Harb. Perspect. Biol.* **5**, a015081 (2013).
4. Y. Kawano, R. Kypta, Secreted antagonists of the Wnt signaling pathway. *J. Cell Sci.* **1**, 2627–2634 (2003).
5. J. C. Hsieh, L. Kodjabachian, M. L. Rebbert, A. Rattner, P. M. Smallwood, C. H. Samos, R. Nusse, I. B. Dawid, J. Nathans, A new secreted protein that binds to Wnt proteins and inhibits their activities. *Nature* **398**, 431–436 (1999).
6. C. Wissmann, P. J. Wild, S. Kaiser, S. Roepcke, R. Stoehr, M. Woenckhaus, G. Kristiansen, J. Hsieh, F. Hofstaedter, A. Hartmann, R. Knuechel, A. Rosenthal, C. Pilarsky, WIF1, a component of the Wnt pathway, is down-regulated in prostate, breast, lung, and bladder cancer. *J. Pathol.* **201**, 204–212 (2003).
7. J. Mazieres, B. He, L. You, Z. Xu, A. Y. Lee, I. Mikami, N. Reguart, R. Rosell, F. McCormick, D. M. Jablons, Wnt inhibitory factor-1 is silenced by promoter hypermethylation in human lung cancer. *Cancer Res.* **64**, 4717–4720 (2004).
8. A. S. Brack, M. J. Conboy, S. Roy, M. Lee, C. J. Kuo, C. Keller, T. A. Rando, Increased Wnt signaling during aging alters muscle stem cell fate and increases fibrosis. *Science* **317**, 807–810 (2007).
9. C. Beyer, A. Schramm, A. Akhmetshina, C. Dees, T. Kireva, K. Gelse, S. Sonnylal, B. de Crombrugghe, M. M. Taketo, O. Distler, G. Schett, J. H. Distler, β-Catenin is a central mediator of pro-fibrotic Wnt signaling in systemic sclerosis. *Ann. Rheum. Dis.* **71**, 761–767 (2012).
10. S. Svegliati, R. Cancello, P. Sambo, M. Luchetti, P. Paroncini, G. Orlandini, G. Discepoli, R. Paternò, M. Santillo, C. Cuozzo, S. Cassano, E. V. Avvedimento, A. Gabrielli, Platelet-derived growth factor and reactive oxygen species (ROS) regulate Ras protein levels in primary human fibroblasts via ERK1/2. Amplification of ROS and Ras in systemic sclerosis fibroblasts. *J. Biol. Chem.* **280**, 36474–36482 (2005).
11. S. S. Baroni, M. Santillo, F. Bevilacqua, M. Luchetti, T. Spadoni, M. Mancini, P. Fraticelli, P. sambo, A. Funaro, A. Kazlauskas, E. V. Avvedimento, A. Gabrielli, Stimulatory auto-antibodies to the PDGF receptor in systemic sclerosis. *N. Engl. J. Med.* **354**, 2667–2676 (2006).
12. Y. Ying, Q. Tao, Epigenetic disruption of the WNT/β-catenin signaling pathway in human cancers. *Epigenetics* **4**, 307–312 (2009).
13. J. Wei, F. Fang, A. P. Lam, J. L. Sargent, E. Hamburg, M. E. Hinchcliff, C. J. Gottardi, R. Atit, M. L. Whitfield, J. Varga, Wnt/β-catenin signaling is hyperactivated in systemic sclerosis and induces Smad-dependent fibrotic responses in mesenchymal cells. *Arthritis Rheum.* **64**, 2734–2745 (2012).
14. L. Ai, Q. Tao, S. Zhong, C. R. Fields, W. Kim, M. W. Lee, Y. Cui, K. D. Brown, K. D. Robertson, Inactivation of Wnt inhibitory factor-1 (WIF1) expression by epigenetic silencing is a common event in breast cancer. *Carcinogenesis* **27**, 1341–1348 (2006).
15. R. Gherzi, M. Trabucchi, M. Ponassi, T. Ruggiero, G. Corte, C. Moroni, C. Y. Chen, K. S. Khabar, J. S. Andersen, P. Briata, The RNA-binding protein KSRP promotes decay of β-catenin mRNA and is inactivated by PI3K-AKT signaling. *PLOS Biol.* **5**, e5 (2006).
16. M. Königshoff, N. Balsara, E. M. Pfaff, M. Kramer, I. Chrobak, W. Seeger, O. Eickelberg, Functional Wnt signaling is increased in idiopathic pulmonary fibrosis. *PLOS One* **3**, e2142 (2008).
17. A. Akhmetshina, K. Palumbo, C. Dees, C. Bergmann, P. Venalis, P. Zerr, A. Horn, T. Kireva, C. Beyer, J. Zwerina, H. Schneider, A. Sadowski, M. Riener, O. A. MacDougald, O. Distler, G. Sheet, J. Distler, Activation of canonical Wnt signaling is required for TGF-β-mediated fibrosis. *Nat. Commun.* **3**, 735 (2012).
18. J. H. Cheng, H. She, Y. Han, J. Wang, S. Xiong, K. Asahina, H. Tsukamoto, Wnt antagonism inhibits hepatic stellate cell activation and liver fibrosis. *Am. J. Physiol. Gastrointest. Liver Physiol.* **294**, G39–G49 (2008).
19. S. Damiano, R. Fusco, A. Morano, M. De Mizio, R. Paternò, A. De Rosa, R. Spinelli, S. Amente, R. Frunzio, P. Mondola, F. Miot, P. Laccetti, M. Santillo, E. V. Avvedimento, Reactive oxygen species regulate the levels of dual oxidase (Duox1-2) in human neuroblastoma cells. *PLOS One* **7**, e34405 (2012).
20. Z. Guo, S. Kozlov, M. F. Lavin, M. D. Person, T. T. Paul, ATM activation by oxidative stress. *Science* **330**, 517–521 (2010).
21. J. Chen, J. Stubbe, Bleomycins: Towards better therapeutics. *Nat. Rev. Cancer* **5**, 102–112 (2005).
22. A. Shibata, O. Barton, A. T. Noon, K. Dahm, D. Deckbar, A. A. Goodarzi, M. Löbrich, P. A. Jeggo, Role of ATM and the damage response mediator proteins 53BP1 and MDC1 in the maintenance of G_2/M checkpoint arrest. *Mol. Cell. Biol.* **30**, 3371–3383 (2010).
23. S. Bhattacharyya, J. Wei, W. G. Tourtellotte, M. Hinchcliff, C. G. Gottardi, J. Varga, Fibrosis in systemic sclerosis: Common and unique pathobiology. *Fibrogenesis Tissue Repair* **5** (Suppl. 1), S18 (2012).
24. H. Noh, E. Y. Oh, J. Y. Seo, M. R. Yu, Y. O. Kim, H. Ha, H. B. Lee, Histone deacetylase-2 is a key regulator of diabetes- and transforming growth factor-β1-induced renal injury. *Am. J. Physiol. Renal Physiol.* **297**, F729–F739 (2009).
25. H. Zhu, L. Shan, P. W. Schiller, A. Mai, T. Peng, Histone deacetylase-3 activation promotes tumor necrosis factor-α (TNF-α) expression in cardiomyocytes during lipopolysaccharide stimulation. *J. Biol. Chem.* **285**, 9429–9436 (2010).
26. N. Koshikawa, J. Hayashi, A. Nakagawara, K. Takenaga, Reactive oxygen species-generating mitochondrial DNA mutation up-regulates hypoxia-inducible factor-1α gene transcription via phosphatidylinositol 3-kinase-Akt/protein kinase C/histone deacetylase pathway. *J. Biol. Chem.* **284**, 33185–33194 (2009).
27. L. C. Huber, J. Distler, F. Moritz, H. Hemmatazad, T. Hauser, B. A. Michel, R. E. Gay, M. Matucci-Cerinic, S. Gay, O. Distler, A. Jüngel, Trichostatin A prevents the accumulation of extracellular matrix in a mouse model of bleomycin-induced skin fibrosis. *Arthritis Rheum.* **56**, 2755–2764 (2007).
28. F. Pacifico, C. Mauro, C. Barone, E. Crescenzi, S. Mellone, M. Monaco, G. Chiappetta, G. Terrazzano, D. Liguoro, P. Vito, E. Consiglio, S. Formisano, A. Leonardi, Oncogenic and anti apoptotic activity of NF-κB in human thyroid carcinomas. *J. Biol. Chem.* **279**, 54610–54619 (2004).
29. M. Bahassi el, S. Karyala, C. R. Tomlinson, M. A. Sartor, M. Medvedovic, R. F. Hennigan, Critical regulation of genes for tumor cell migration by AP-1. *Clin. Exp. Metastasis* **21**, 293–304 (2004).
30. F. Talotta, T. Mega, G. Bossis, L. Casalino, J. Basbous, I. Jariel-Encontre, M. Piechaczyk, P. Verde, Heterodimerization with Fra-1 cooperates with the ERK pathway to stabilize c-Jun in response to the RAS oncoprotein. *Oncogene* **29**, 4732–4740 (2010).
31. T. Hai, C. D. Wolfgang, D. K. Marsee, A. E. Allen, U. Sivaprasad, ATF3 and stress responses. *Gene Expr.* **7**, 321–335 (1999).
32. K. Y. Chung, A. Agarwal, I. Uitto, A. Mauviel, An AP-1 binding sequence is essential for regulation of the human α2(I) collagen (COL1A2) promoter activity by transforming growth factor-β. *J. Biol. Chem.* **271**, 3272–3278 (1996).
33. A. K. Ghosh, Factors involved in the regulation of type I collagen gene expression: Implication in fibrosis. *Exp. Biol. Med.* **227**, 301–314 (2002).
34. S. Morton, R. J. Davis, A. McLaren, P. Cohen, A reinvestigation of the multisite phosphorylation of the transcription factor c-Jun. *EMBO J.* **22**, 3876–3886 (2003).
35. M. Vinciguerra, I. Esposito, S. Salzano, A. Madeo, G. Nagel, M. Maggiolini, A. Gallo, A. M. Musti, Negative charged threonine 95 of c-Jun is essential for c-Jun N-terminal kinase-dependent phosphorylation of threonine 91/93 and stress-induced c-Jun biological activity. *Int. J. Biochem. Cell Biol.* **40**, 307–316 (2008).
36. C. E. Reddy, L. Albaniro, P. De Marco, D. Aiello, M. Maggiolini, A. Napoli, A. M. Musti, Multisite phosphorylation of c-Jun at threonine 91/93/95 triggers the onset of c-Jun pro/apoptotic activity in cerebellar granule neurons. *Cell Death Dis.* **4**, e852 (2013).
37. Y. Tanaka, A. Nakamura, M. S. Morioka, S. Inoue, M. Tamamori-Adachi, K. Yamada, K. Taketani, J. Kawauchi, M. Tanaka-Okamoto, J. Miyoshi, H. Tanaka, S. Kitajima, Systems analysis of ATF3 in stress response and cancer reveals opposing effects on pro-apoptotic genes in p53 pathway. *PLOS One* **6**, e26848 (2011).
38. M. Cebrat, L. Strzadala, P. Kisielow, Wnt inhibitory factor-1: A candidate for a new player in tumorigenesis of intestinal epithelial cells. *Cancer Lett.* **206**, 107–113 (2004).
39. J. W. Wen, J. T. Hwang, G. M. Kelly, Reactive oxygen species and Wnt signalling crosstalk patterns mouse extraembryonic endoderm. *Cell. Signal.* **24**, 2337–2348 (2012).
40. Z. Guo, R. Deshpande, T. Paull, ATM activation in the presence of oxidative stress. *Cell Cycle* **9**, 4805–4811 (2010).
41. C. Cosentino, D. Grieco, V. Costanzo, ATM activates the pentose phosphate pathway promoting anti-oxidant defence and DNA repair. *EMBO J.* **30**, 546–555 (2011).
42. A. Gabrielli, E. V. Avvedimento, T. Krieg, Scleroderma. *N. Engl. J. Med.* **360**, 1989–2003 (2009).
43. L. A. Rowe, N. Degtyareva, P. W. Doetsch, DNA damage-induced reactive oxygen species (ROS) stress response in *Saccharomyces cerevisiae*. *Free Radic. Biol. Med.* **45**, 1167–1177 (2008).
44. D. Lallemand, G. Spyrou, M. Yaniv, C. M. Pfarr, Variations in Jun and Fos protein expression and AP-1 activity in cycling, resting and stimulated fibroblasts. *Oncogene* **14**, 819–830 (1997).
45. Y. Chinenov, T. Kerppola, Close encounters of many kinds: Fos-Jun interactions that mediate transcription regulatory specificity. *Oncogene* **20**, 2438–2452 (2001).
46. L. Shu, K. C. Shen, Y. Wang, S. C. Brooks, Y. A. Wang, Impaired hepatocyte survival and liver regeneration in Atm-deficient mice. *Hum. Mol. Genet.* **14**, 3019–3025 (2005).
47. G. Liang, C. D. Wolfgang, B. P. Chen, T. H. Chen, T. Hai, *ATF3* gene. Genomic organization promoter, and regulation. *J. Biol. Chem.* **271**, 1695–1701 (1996).
48. K. Toualbi, M. C. Güller, J. L. Mauriz, C. Labalette, M. A. Buendia, A. Mauviel, D. Bernuau, Physical and functional cooperation between AP-1 and β-catenin for the regulation of TCF-dependent genes. *Oncogene* **26**, 3492–3502 (2007).
49. A. L. Delmas, B. M. Riggs, C. E. Pardo, L. M. Duer, R. P. Darst, E. G. Izumchenko, M. Monroe, A. Hakam, M. P. Kladde, E. M. Siegel, K. D. Brown, *WIF1* is a frequent target for epigenetic silencing in squamous cell carcinoma of the cervix. *Carcinogenesis* **32**, 1625–1633 (2011).
50. M. Kansara, M. Tsang, L. Kodjabachian, N. A. Sims, M. K. Trivett, M. Ehrich, A. Dobrovic, J. slavin, P. F. Choong, P. J. Simmons, I. B. Dawid, D. M. Thomas, Wnt inhibitory factor 1 is epigenetically silenced inhuman osteosarcoma, and targeted disruption accelerates osteosarcomagenesis in mice. *J. Clin. Invest.* **119**, 837–851 (2009).
51. E. V. Avvedimento, S. Obici, M. Sanchez, A. Gallo, A. Musti, M. E. Gottesman, Reactivation of thyroglobulin gene expression in transformed thyroid cells by 5-azacytidine. *Cell* **58**, 1135–1142 (1989).

52. B. L. Vaes, K. J. Dechering, E. P. van Someren, J. M. Hendriks, C. J. van de Ven, A. Feijen, C. L. Mummery, M. J. Reinders, W. Olijve, E. J. van Zoelen, W. T. Steegenga, Microarray analysis reveals expression regulation of Wnt antagonists in differentiating osteoblasts. *Bone* **36**, 803–811 (2005).
53. M. Bocchino, S. Agnese, E. Fagone, S. Svegliati, D. Grieco, C. Vancheri, A. Gabrielli, A. Sanduzzi, E. V. Avvedimento, Reactive oxygen species are required for maintenance and differentiation of primary lung fibroblasts in idiopathic pulmonary fibrosis. *PLOS One* **5**, e14003 (2010).
54. D. Y. Zhang, Y. Pan, C. Zhang, B. X. Yan, S. S. Yu, D. L. Wu, M. M. Shi, K. Shi, X. X. Cai, S. S. Zhou, J. B. Wang, J. P. Pan, L. H. Zhang, Wnt/β-catenin signaling induces the aging of mesenchymal stem cells through promoting the ROS production. *Mol. Cell. Biochem.* **374**, 13–20 (2013).
55. A. Milano, S. A. Pendergrass, J. L. Sargent, L. K. George, T. H. McCalmont, M. K. Connolly, M. L. Whitfield, Molecular subsets in the gene expression signatures of scleroderma skin. *PLOS One* **3**, e2696 (2008).
56. D. Wu, P. Wong, W. Li, C. F. Vogel, F. Matsumura, Suppression of *WIF-1* through promoter hypermethylation causes accelerated proliferation of the aryl hydrocarbon receptor (AHR) overexpressing MCF10AT1 breast cancer cells. *Toxicology* **285**, 97–103 (2011).
57. J. Behari, The Wnt/β-catenin signaling pathway in liver biology and disease. *Expert Rev. Gastroenterol. Hepatol.* **4**, 745–759 (2010).
58. M. Bonifazi, I. Tramacere, G. Pomponio, B. Gabrielli, E. V. Avvedimento, C. La Vecchia, E. Negri, A. Gabrielli, Systemic sclerosis (scleroderma) and cancer risk: Systematic review and meta-analysis of observational studies. *Rheumatology* **52**, 143–154 (2013).

Acknowledgments: We thank P. Verde for the AP1 expression vectors, M. L. Bocchino for primary cultures isolated from idiopathic lung fibrosis patients, A. Leonardi for the NF-κB repressor-expressing vector (*25*), and S. Saccomanno for the human histological sections. **Funding:** This work was supported by a Young Investigator Award from Gruppo Italiano Lotta alla Sclerodermia to G.M., by grants from Ministero Italiano per l'Università e la Ricerca Scientifica, Fondazione Cariverona, Fondazione Italiana Ricerca Artrite, Fondazione di Medicina Molecolare e Terapia Cellulare, Università Politecnica delle Marche, Ancona, Italy, and from Associazione Italiana Ricerca sul Cancro (AIRC) IG. 11364, from Epigenomics Flagship Project—EPIGEN to C.N.R., and from POR Campania FSE 2007-2013, Project CRÈME. **Author contributions:** G. Marrone and A.P. carried out the ChIP assays, the analysis of AP1 transcription factors, posttranscriptional modifications, and transfections. S.A. performed the immunohistological and immunofluorescence experiments. S.S. performed Western blot assays, interpreted results, and assisted in manuscript preparation. T.S. performed the cellular assays and RT-PCR. A.J. and O.D. provided the mouse histological sections. A. Grieco and G. Moroncini contributed to primer design and experiments using recombinant SSc-IgG. D.G. and M.V. conducted the experiments with A-T cells. A.M.M. supervised the experiments with AP1 transcription factors and generated the c-Jun mutants. A. Gabrielli and E.V.A. supervised the project and wrote the manuscript. **Competing interests:** The authors declare that they have no competing interests.

Submitted 5 August 2013
Accepted 28 July 2014
Final Publication 2 September 2014
10.1126/scisignal.2004592
Citation: S. Svegliati, G. Marrone, A. Pezone, T. Spadoni, A. Grieco, G. Moroncini, D. Grieco, M. Vinciguerra, S. Agnese, A. Jüngel, O. Distler, A. M. Musti, A. Gabrielli, E. V. Avvedimento, Oxidative DNA damage induces the ATM-mediated transcriptional suppression of the Wnt inhibitor WIF-1 in systemic sclerosis and fibrosis. *Sci. Signal.* **7**, ra84 (2014).